IPHE 2002-03

B Physics at LHC(b)

T. Nakada
CERN, CH-1211 Geneva 23, Switzerland
and
IPHE, Université de Lausanne, CH-1015 Lausanne, Switzerland

Lecture given at
A NATO Advanced Study Institute
55th Scottish Universities Summer School in Physics
"Heavy Flavour Physics"
7- 23 August 2001, St. Andrews, Scotland

February 7, 2002

1 Introduction

Since its discovery, the b quark brought us two big surprises. The first surprise was the unexpectedly large lifetime. The second one was that the mass difference between the two mass eigenstates of the B_d meson system is $\sim$100 times larger than the similar mass difference in the neutral K meson system. From the first observation, we learned that the mixing between the second and third families is much smaller than that between the first and second families. (The mixing between the first and third families is even more suppressed.) The second one taught us that the mass of the top quark is much larger than anticipated at that time.

The main goal of B physics is to study the structure of the quark mixing and its role in CP violation. CP violation can be very naturally accommodated in the Standard Model [1] through the complex quark mixing matrix

defined by four parameters and all the currently observed CP violation phenomena in particle physics are in full agreement with the Standard Model calculations. However, there are still some reasons to speculate about CP violation generated by physics beyond the Standard Model. Firstly, the Standard Model alone cannot account for the large asymmetry between matter and antimatter observed in our universe [2]. Secondly, various types of extension to the Standard Model introduce new sources of CP violation. Since CP violation is expected in many B meson decay modes and the Standard Model can make precise predictions for some of those decay modes, the B meson system appears to be a very attractive place to look for evidence beyond the Standard Model.

With the presence of New Physics, some assumptions made to extract the CKM parameters are no longer valid. Indeed, the consistency of the CKM picture currently seen could be accidental due a numerical cancellation between various effects from New Physics and that from the Standard Model. Therefore, it is essential to develop a strategy which allows the New Physics and the Standard Model contributions to be clearly disentangled. Then, the CKM parameters can be determined in a model-independent way. This is also important since we hope that physics at higher energy scale would one day be able to explain the family structure, by deriving the CKM parameters.

In this article, we discuss how B meson decays can be explored in order to obtain a better understanding of the CKM picture and to look for physics beyond the Standard Model.

2 CKM Picture

2.1 The CKM Matrix

In the Standard Model, CP violation is naturally introduced by the 3×3 complex Cabibbo-Kobayashi-Maskawa (CKM) quark mixing matrix, V, expressed as

$$V = \begin{pmatrix} V_{\rm ud} & V_{\rm us} & V_{\rm ub} \\ V_{\rm cd} & V_{\rm cs} & V_{\rm cb} \\ V_{\rm td} & V_{\rm ts} & V_{\rm tb} \end{pmatrix} .$$

The charged current of the weak interaction is then proportional to

$$\overline{U}^i_{\rm L} \left(1 - \gamma_5\right) \gamma_\mu V_{ij} D^j_{\rm L} W^{+\mu}$$

where $U_{\rm L}$ and $D_{\rm L}$ are the left-handed quark operators for the charge 2/3 up-type and the charge $-1/3$ down-type quarks respectively: i.e.

$$U_{\rm L} = \begin{pmatrix} u_{\rm L} \\ c_{\rm L} \\ t_{\rm L} \end{pmatrix}, \text{ and } D_{\rm L} = \begin{pmatrix} d_{\rm L} \\ s_{\rm L} \\ b_{\rm L} \end{pmatrix} .$$

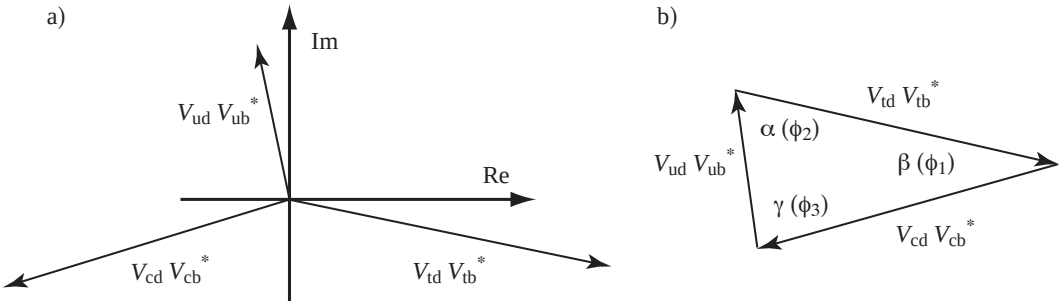

Figure 1: a) One of the unitarity conditions of the CKM matrix, $V_{\rm ud}V_{\rm ub}^* + V_{\rm cd}V_{\rm cb}^* + V_{\rm td}V_{\rm tb}^* = 0$ drawn in the complex plane. b) Elements transported so that a triangle can be formed.

The matrix V is unitary, i.e. $V^\dagger V = 1$. One of the unitarity relations

$$V_{\rm ud}V_{\rm ub}^* + V_{\rm cd}V_{\rm cb}^* + V_{\rm td}V_{\rm tb}^* = 0 \tag{1}$$

is illustrated in Figure 1-a in the complex plane. The unitarity condition can be illustrated easily by transporting $V_{\rm cd}V_{\rm cb}^*$ and $V_{\rm td}V_{\rm tb}^*$ so that a closed triangle is formed, as shown in Figure 1-b. Three angles of the triangle, α, β and γ (also known as ϕ_2, ϕ_1 and ϕ_3 respectively) can be defined as

$$\alpha = \tan^{-1}\frac{-V_{\rm td}V_{\rm tb}^*}{V_{\rm ud}V_{\rm ub}^*},\ \beta = \pi - \tan^{-1}\frac{V_{\rm td}V_{\rm tb}^*}{V_{\rm cd}V_{\rm cb}^*},\ \gamma = \tan^{-1}\frac{-V_{\rm ud}V_{\rm ub}^*}{V_{\rm cd}V_{\rm cb}^*} . \tag{2}$$

It should be noted that a redefinition of the quark phases results in a rotation of the triangle while the three angles, α, β and γ remain invariant.

Violation of the unitarity condition given by Equation 1 is expressed in a graphical form in Figure 2-a and -b, where the three sides given by $V_{\rm ud}V_{\rm ub}^*$, $V_{\rm cd}V_{\rm cb}^*$ and $V_{\rm td}V_{\rm tb}^*$ do not form a closed triangle. Note that α, β and γ defined as Equations 2 still fulfill

$$\alpha + \beta + \gamma = \pi .$$

If one forms the closed triangle from the length of the three sides, $|V_{\rm ud}V_{\rm ub}^*|$, $|V_{\rm cd}V_{\rm cb}^*|$ and $|V_{\rm td}V_{\rm tb}^*|$, the three angles of this triangle, α', β' and γ' defined as in Figure 2-c, are not identical to α, β and γ. Therefore, a test of the unitarity can be made by comparing the angles defined by the length of the three sides and α, β or γ measured by CP violation as explained later.

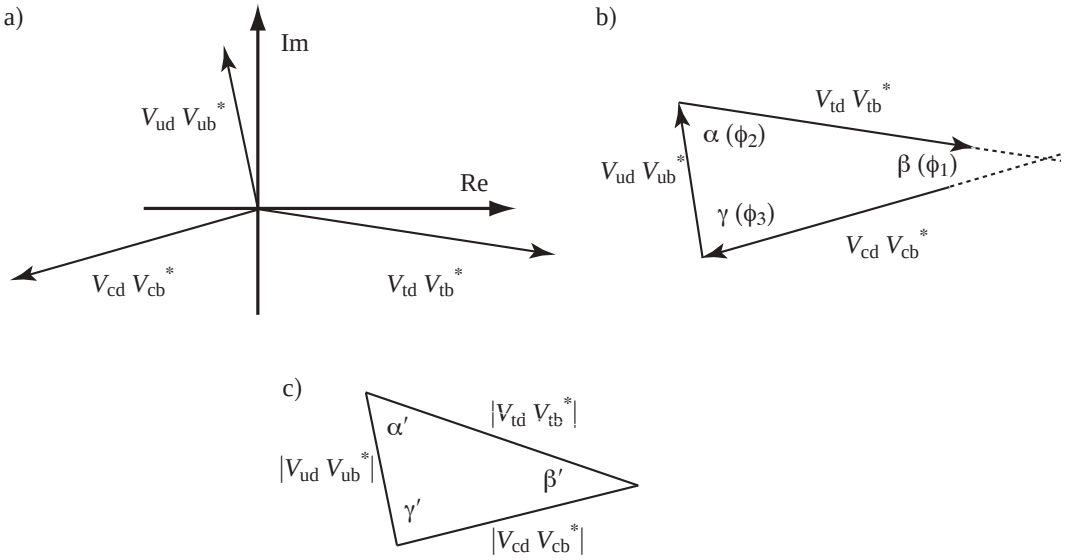

Figure 2: a) and b), are similar to Figure 1, however unitarity is violated. In c) a closed triangle is formed using the three sides.

A unitary 3×3 matrix can be parameterized by four parameters. One possible choice [3] is to use the three angles and one phase, θ_{12}, θ_{23}, θ_{13} and δ respectively. Then the "standard" parameterization for the CKM matrix can be given by

$$V = R_{23} \times R_{13} \times R_{12}$$

where

$$R_{12} = \begin{pmatrix} c_{12} & s_{12} & 0 \\ -s_{12} & c_{12} & 0 \\ 0 & 0 & 1 \end{pmatrix}, R_{23} = \begin{pmatrix} 1 & 0 & 0 \\ 0 & c_{23} & s_{23} \\ 0 & -s_{23} & c_{23} \end{pmatrix}, R_{13} = \begin{pmatrix} c_{13} & 0 & s_{13}e^{-i\,\delta} \\ 0 & 1 & 0 \\ -s_{13}e^{i\,\delta} & 0 & c_{13} \end{pmatrix}$$

with $s_{ij} = \sin\theta_{ij}$ and $c_{ij} = \cos\theta_{ij}$.

A parametrization reflecting the observed pattern of the CKM matrix was first proposed by Wolfenstein [4]. First, we introduce the following transfor-

mation,

$$\lambda = \sin\theta_{12}, A = \frac{s_{23}}{s_{12}^2}, \rho = \frac{s_{13}\cos\delta}{s_{12}s_{23}}, \eta = \frac{s_{13}\sin\delta}{s_{12}s_{23}},$$

then expand the elements in powers of λ. By neglecting terms proportional to λ^n where $n > 5$, we obtain

$$V \approx \begin{pmatrix} 1-\lambda^2/2 & \lambda & A\lambda^3(\rho - i\,\eta) \\ -\lambda - i\,A^2\lambda^5\eta & 1-\lambda^2/2 & A\lambda^2 \\ A\lambda^3(1-\tilde{\rho}-i\,\tilde{\eta}) & -A\lambda^2 - i\,A\lambda^4\eta & 1 \end{pmatrix}, \qquad (3)$$

where $\tilde{\rho}$ and $\tilde{\eta}$ are given by $\tilde{\rho} = \rho(1-\lambda^2/2)$ and $\tilde{\eta} = \eta(1-\lambda^2/2)$. The parameter λ is known from light hadron decays to be 0.221 ± 0.002 [3]. As seen from Equation 3, the first 2×2 sub-matrix is almost unitary, i.e.

$$V_{\rm ud}V_{\rm cd}^* + V_{\rm us}V_{\rm cs}^* = iA^2\lambda^5\eta \approx 0,\ V_{\rm ud}V_{\rm us}^* + V_{\rm cd}V_{\rm cs}^* = -iA^2\lambda^5\eta \approx 0$$

and

$$|V_{\rm ud}|^2 + |V_{\rm us}|^2 = 1 - \lambda^4/4 \approx 1,\ |V_{\rm cd}|^2 + |V_{\rm cs}|^2 = 1 - \lambda^4/4 \approx 1.$$

With the parametrization given in Equation 3, the imaginary part of $V_{\rm cd}$ becomes negligible in the unitarity relation given by Equation 1. The phases of the elements those appear in the equation are given by

$$\arg V_{\rm td} = -\beta,\ \arg V_{\rm ub} = -\gamma,\ \arg V_{\rm ud} = \arg V_{\rm cb} = \arg V_{\rm tb} = 0 \text{ and } \arg V_{\rm cd} = \pi.$$

The imaginary part of $V_{\rm ts}$ cannot be ignored and

$$\arg V_{\rm ts} = \delta\gamma + \pi$$

where β, γ and and $\delta\gamma$ are determined by ρ, η and λ as

$$\beta = \tan^{-1}\frac{\eta}{1-\rho},\ \gamma = \tan^{-1}\frac{\eta}{\rho},\ \delta\gamma = \tan^{-1}\lambda^2\eta\ . \qquad (4)$$

2.2 Extraction of the CKM Parameters

The element $|V_{\rm cb}|$ is extracted from both semileptonic and hadronic decays of B mesons into charmed mesons final states. In the actual B meson decays, a description based on the quark level tree process $\rm b \to c + W^-$ is obscured by the soft hadronic interactions. This effect has to be taken into account

in order to extract $|V_{\rm cb}|$ from the data. Significant improvements in theory and experiment to understand this hadronic effect have been made. Further progress will continue thanks to the high statistics data from the BABAR and BELLE experiments. From $|V_{\rm cb}|$, the parameter A can be determined.

For the $|V_{\rm ub}|$ extraction, the semileptonic decays of B meson with the final states containing only light quarks (i.e. u and d) are used. They are generated by the $\rm b \to u + W^-$ tree process. Unlike for the determination of $|V_{\rm cb}|$, hadronic decays cannot be used since sizeable contributions from the penguin processes, $\rm b \to s$ and $\rm b \to d$, are present in the decay amplitudes. Difficulties in evaluating the effect of strong interactions is also much more daunting than for $|V_{\rm cb}|$. The error on the current value of $|V_{\rm ub}|$ is totally dominated by the theoretical uncertainties and this will remain the case for some time.

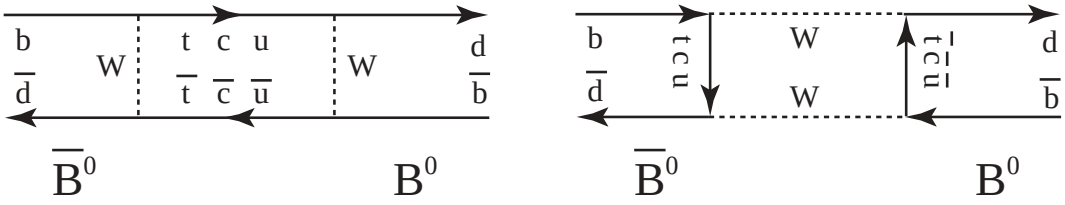

Figure 3: Box diagrams describing $\rm B^0$-$\overline{\rm B}^0$ oscillation.

While $|V_{\rm cb}|$ and $|V_{\rm ub}|$ are determined from decays with tree processes, $|V_{\rm td}|$ can be accessed "indirectly" through loop processes such as $\rm B^0$-$\overline{\rm B}^0$ oscillations. The oscillation in the Standard Model is described by the well known box diagrams shown in Figure 3. Due to the large top quark mass and the structure of the CKM matrix, only the top quark contribution needs to be considered in the loop. By neglecting the absorptive part of the box diagrams, the oscillation amplitude for $\rm B^0 \to \overline{B}^0$ is calculated to be [5]

$$H_{21}^{\rm d} = -\frac{G_{\rm F}^2 f_{\rm B_d}^2 B_{\rm B_d} m_{\rm B_d} m_{\rm W}^2}{12\pi^2} \eta_{\rm B_d} S(x_{\rm t}) (V_{\rm td} V_{\rm tb}^*)^2 \qquad (5)$$

where $G_{\rm F}$, $m_{\rm W}$ and $m_{\rm B_d}$ are the Fermi coupling constant, mass of the W boson and mass of the $\rm B_d$ meson respectively, which are well measured. The known function $S(x_{\rm t})$ is determined from the mass ratio, $x_{\rm t} = (m_{\rm t}/m_{\rm W})^2$ where $m_{\rm t}$ is the top quark mass, and the QCD correction $\eta_{\rm B_d}$ can be calculated reliably with perturbation method. The decay constant, $f_{\rm B_d}$, and the

B-parameter, $B_{\mathrm{B_d}}$, have never been measured and only theoretical estimates exist with large uncertainties due to difficulties in evaluating the effect of the non-perturbative soft hadronic interactions. The most promising theoretical approach to obtain $f_{\mathrm{B_d}}$ and $B_{\mathrm{B_d}}$ is the QCD lattice calculation discussed in these proceedings. The decay constant $f_{\mathrm{B_d}}$ is given by the transition matrix element between B^0 and the hadronic vacuum state, thus could be experimentally obtained once the branching fraction for the leptonic decay, $\mathrm{B}^{\pm} \to \tau^{\pm}\nu_{\tau}$ shown in Figure 4, becomes known (assuming that $|V_{\mathrm{ub}}|$ is measured). The decay constants for $\mathrm{B}^{\pm}$ and B^0 are expected to be very similar. The B-parameter takes into account the difference between the hadronic vacuum and the actual hadronic states virtually present in the B^0-$\overline{\mathrm{B}}^0$ oscillation processes.

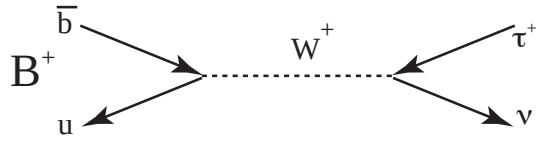

Figure 4: Diagram for the $\mathrm{B}^+ \to \tau^+\nu_{\tau}$ decay.

The absorptive part in the B^0-$\overline{\mathrm{B}}^0$ oscillation due to c- and u-quarks is calculated to be very small compared to the dispersive part and can indeed be ignored. With this approximation, the mass difference between the two mass eigenstates, $\mathrm{B_d^{heavy}}$ and $\mathrm{B_d^{light}}$, can be derived as

$$\Delta m_{\mathrm{d}} \equiv m_{\mathrm{B_d^{heavy}}} - m_{\mathrm{B_d^{light}}} = 2|H_{21}^{\mathrm{d}}| \ .$$

and the decay width difference between them is zero, i.e.

$$\Delta\Gamma_{\mathrm{d}} \equiv \Gamma_{\mathrm{B_d^{light}}} - \Gamma_{\mathrm{B_d^{heavy}}} = 0 \ .$$

There is no CP violation in the B^0-$\overline{\mathrm{B}}^0$ oscillations in this approximation. Note that the phase of the oscillation amplitude is given by the phase of V_{td}^2 and is -2β.

The mass difference Δm_{d} is experimentally measured as the frequency of the B^0-$\overline{\mathrm{B}}^0$ oscillation. From the known structure of the CKM matrix, we have $|V_{\mathrm{tb}}| = 1$ with very high accuracy. Therefore, $|V_{\mathrm{td}}|$ can be obtained from Δm_{d}. The error on $|V_{\mathrm{td}}|$ is totally dominated by the theoretical uncertainties on $f_{\mathrm{B}}\sqrt{B_{\mathrm{d}}}$.

Now,

$$\sqrt{\tilde{\rho}^2 + \tilde{\eta}^2} = \frac{|V_{\rm ub}|}{\lambda |V_{\rm cb}|} \left(1 - \frac{\lambda^2}{2}\right) \tag{6}$$

and

$$\sqrt{(1-\tilde{\rho})^2 + \tilde{\eta}^2} = \frac{|V_{\rm td}|}{\lambda |V_{\rm cb}|} \tag{7}$$

can be drawn as circles around (0, 0) and (1, 0) in the $\tilde{\rho}$-$\tilde{\eta}$ plane respectively. Among the two possible solutions, $\eta > 0$ is favoured from the analysis of CP violation in the $\rm K^0$-$\overline{\rm K}^0$ oscillations.

Similar to the $\rm B^0$ meson, the mass difference in the $\rm B_s$ system, $\Delta m_{\rm s}$, can be evaluated by calculating the $\rm B_s^0$-$\overline{\rm B}_s^0$ oscillation amplitude using box diagrams and it determines $|V_{\rm ts} V_{\rm tb}^*|^2$. Once $\Delta m_{\rm s}$ is measured,

$$\sqrt{(1-\tilde{\rho})^2 + \tilde{\eta}^2} = \frac{|V_{\rm td}|}{\lambda |V_{\rm ts}|} \tag{8}$$

can be used instead of Equation 7. It follows that

$$\frac{|V_{\rm td}|}{\lambda |V_{\rm ts}|} = \frac{\sqrt{\Delta m_{\rm d}}}{\lambda \sqrt{\Delta m_{\rm d}}} \times \frac{\sqrt{m_{\rm B_s} \eta_{\rm B_s}}}{\sqrt{m_{\rm B_d} \eta_{\rm B_d}}} \times \frac{\sqrt{B_{\rm B_s}} f_{\rm B_s}}{\sqrt{B_{\rm B_d}} f_{\rm B_d}} \ ,$$

where the assumption $|V_{\rm tb}| = 1$ is no longer necessary. While the theoretical uncertainty in $f_B \sqrt{B}$ is quite considerable, the ratio between them for the $\rm B_s^0$ and $\rm B^0$ mesons is theoretically much better understood. Therefore, Equation 8 will have significantly smaller error than Equation 7. Unfortunately, only a lower limit is known for $\Delta m_{\rm s}$ at the moment.

We now consider CP violation for the decay final states which could be produced by both $\rm B^0$ and $\overline{\rm B}^0$. They could be CP eigenstates such as $\rm J/\psi\, K_S$ or CP non-eigenstates such as $\rm D^{*+}\pi^-$ and its CP-conjugated state $\rm D^{*-}\pi^+$. If CP violation is present in neither the oscillation nor the decay amplitudes, it is well-known that the signature of CP violation appears only as

$$\sin(\phi_{\rm oscillation} + \phi_{\rm decay}) \sin(\Delta m_{\rm d} t)$$

in the time-dependent decay rates of initial $\rm B^0$ and $\overline{\rm B}^0$, where $\phi_{\rm oscillation}$ is the phase of the $\rm B^0$-$\overline{\rm B}^0$ oscillation amplitude and $\phi_{\rm decay}$ is the phase of the ratio of the instantaneous decay amplitudes of $\rm B^0$ and $\overline{\rm B}^0$ into the considered final state.

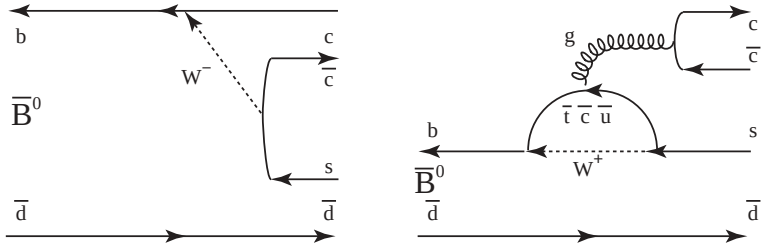

Figure 5: Quark diagrams for the $\overline{\mathrm{B}}^0 \to \mathrm{J}/\psi\,\mathrm{K_S}$ decay.

For the $\mathrm{J}/\psi\,\mathrm{K_S}$ final state, both $\mathrm{b} \to \mathrm{c} + \mathrm{W}^-$ tree process and $\mathrm{b} \to \mathrm{s}$ penguin process (shown in Figure 5) contribute to the decay. The phase of the tree process is given by V_{cb} which is 0 in the Wolfenstein's approximation, given in Equation 3. The penguin process is dominated by the virtual top quark with corresponding CKM matrix elements, $V_{\mathrm{tb}}V_{\mathrm{ts}}^*$, which has only a small phase $-\delta\gamma$. Therefore, $\phi_{\mathrm{decay}} = 0$ with a theoretical uncertainty less than a few percent.

The final state $\mathrm{D}^{*+}\pi^-$ can be generated by the tree process $\mathrm{b} \to \mathrm{c} + \mathrm{W}^-$, followed by $\mathrm{W}^- \to \overline{\mathrm{u}}\mathrm{d}$ for the $\overline{\mathrm{B}}^0$ decay or $\overline{\mathrm{b}} \to \overline{\mathrm{u}} + \mathrm{W}^+$ followed by $\mathrm{W}^+ \to \mathrm{c}\overline{\mathrm{d}}$ for the B^0 decay, as seen from Figure 6. From the relevant CKM matrix elements, it follows that $\phi_{\mathrm{decay}} = \gamma$. Note that only the tree processes contribute.

The phase of the oscillation amplitude is given by 2β as discussed before. Therefore, CP violation signatures in B^0 and $\overline{\mathrm{B}}^0$ decays are

$$\sin(2\beta)\sin\left(\Delta m_{\mathrm{d}} t\right) \quad \text{for} \quad \mathrm{J}/\psi\,\mathrm{K_S}$$

and

$$\sin(2\beta+\gamma)\sin\left(\Delta m_{\mathrm{d}} t\right) \quad \text{for} \quad \mathrm{D}^{*+}\pi^- \text{ and } \mathrm{D}^{*-}\pi^+ \ .$$

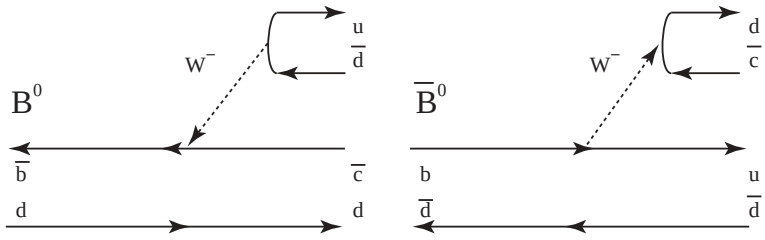

Figure 6: Quark diagrams for the B^0 and $\overline{\mathrm{B}}^0 \to \mathrm{D}^{*+}\pi^-$ decays.

For the $\sin(2\beta)$ measurement, averaging the recent results by BABAR and BELLE provides [6]

$$\sin 2\beta = 0.79 \pm 0.17$$

where the error is scaled following the recipe of the Particle Data Group. It is unlikely that any definitive measurement on $\sin(2\beta + \gamma)$ will be done by the current generation of experiments.

Analogous decays for the B_s^0 meson system are $J/\psi\,\phi$ (or $J/\psi\,\eta$) which give $\phi_{\rm decay} = 0$ and $D_s^+K^-$ with $\phi_{\rm decay} = \gamma$. Since the B_s^0-$\overline{B}_s^0$ oscillation phase is $-2\delta\gamma$ as discussed before, the CP violation signature would be given by

$$\sin(-2\delta\gamma)\sin(\Delta m_s t) \quad \text{for} \quad J/\psi\,\phi \ (\text{or } J/\psi\,\eta)$$

and

$$\sin(-2\delta\gamma+\gamma)\sin(\Delta m_s t) \quad \text{for} \quad D_s^+K^- \text{ and } D_s^-K^+ \ .$$

No definitive measurements on both of these quantities will be available from the current generation of the experiments.

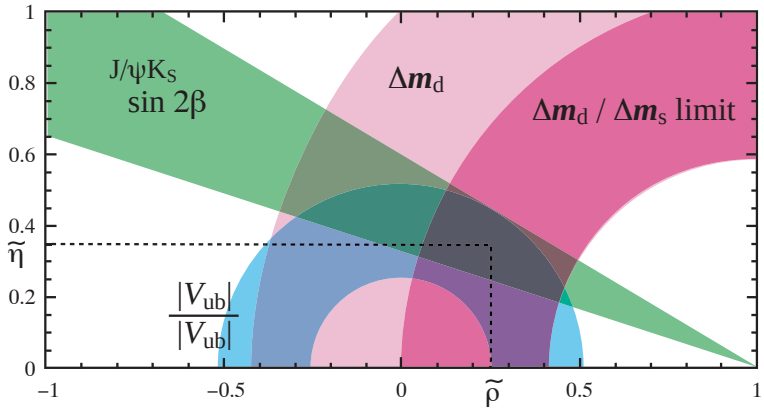

Figure 7: Allowed region in the $\tilde{\rho}$-$\tilde{\eta}$ plane by the Standard Model analysis on $|V_{\rm ub}|/(\lambda|V_{\rm cb}|)$, $\Delta m_{\rm d}$, an upper limit on $\Delta m_{\rm s}$ and $\sin(2\beta)$ measurements currently available.

In Figure 7, we summarise the region of $\tilde{\rho}$ and $\tilde{\eta}$ allowed by the current data on $|V_{\rm ub}|/(\lambda|V_{\rm cb}|)$, $\Delta m_{\rm d}$, $\Delta m_{\rm d}/\Delta m_{\rm s}$ constrained by lower limit on $\Delta m_{\rm s}$ and $\sin(2\beta)$. As explained, data are interpreted within the framework of the Standard Model. There is a common overlapping region indicating that

the data are consistent with the CKM picture and no sign of New Physics is visible within the errors. Note that the $\sin(2\beta)$ measurement gives two allowed regions in the $\tilde{\rho}$-$\tilde{\eta}$ plane defined in Figure 7. Only one of them is drawn.

3 Possible CKM Picture in 2006

Let us now speculate about the CKM landscape in 2006. Due to progress in theoretical understanding of the hadronic effect, strongly helped by the large statistics and high quality data by BABAR and BELLE, $|V_{ub}/V_{cb}|$ might become known with a relative error of $\pm 10\%$. Once Δm_s is measured by CDF, $|V_{td}|/(\lambda|V_{ts}|)$ will become known with a relative error of $\pm 7\%$. From the CP violation in B^0 and $\overline{B}^0$ decaying into $J/\psi\, K_S$, combined results from BABAR, BELLE, CDF and D0 might yield a result of $\sin(2\beta)$ with an error as small as 0.03, which is still statistically limited. Estimating the progress in other CP violation channels is more difficult since they have various theoretical uncertainties where future improvements are difficult to evaluate. Assuming that the currently preferred values of ρ and η remain unchanged, the situation expected in 2006 is illustrated in Figure 8.

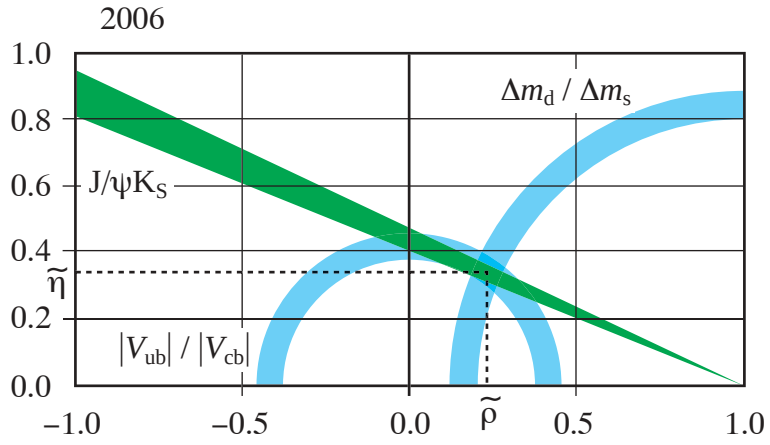

Figure 8: Possible situation of the allowed region in the $\tilde{\rho}$-$\tilde{\eta}$ plane in 2006

4 Presence of New Physics

Once we allow the presence of physics beyond the Standard Model, determination of the CKM matrix elements becomes much more complicated. Most of the extensions of the Standard Model introduce new heavy particles. Due to the mass, their contribution to the tree processes should be negligible. For B^0-$\overline{B}^0$ and B_s^0-$\overline{B}_s^0$ oscillations, their contribution in the box processes could be still sizeable. New heavy particles could appear in the penguin processes as well. However, their effect should be much less than in the box processes due to the different dependences on the masses of the particles appearing in the loops for the two processes.

With the presence of New Physics, the phase of the B^0-$\overline{B}^0$ oscillation amplitude is modified to be

$$\phi^{\rm d}_{\rm oscillation} = 2\beta + \phi^{\rm d}_{\rm NP}$$

and

$$\phi^{\rm s}_{\rm oscillation} = -2\delta\gamma + \phi^{\rm s}_{\rm NP}$$

for the B_s^0-$\overline{B}_s^0$ oscillation amplitude, where $\phi^{\rm d}_{\rm NP}$ and $\phi^{\rm s}_{\rm NP}$ are due to New Physics.

New Physics can affect very little the decay amplitude generated by the tree processes. Therefore, we assume that the phase of the amplitudes for decay modes such as $B^0 \to J/\psi\, K_S$, $B^0 \to D^{*+}\pi^-$, $B_s^0 \to J/\psi\,\phi$ and $B_s^0 \to D_s^+ K^-$ would remain unchanged.

From the CP violation signature in B^0 and $\overline{B}^0$ decays, we would then have

$$\sin(2\beta + \phi^{\rm d}_{\rm NP}) \sin \Delta m_{\rm d} t \quad \text{for} \quad J/\psi\, K_S \tag{9}$$

and

$$\sin(2\beta + \phi^{\rm d}_{\rm NP} + \gamma) \sin \Delta m_{\rm d} t \quad \text{for} \quad D^{*+}\pi^- \text{ and } D^{*-}\pi^+.$$

This allow us to extract the angle, γ, in a theoretically clean way, even if New Physics is present.

Similarly for the B_s^0-meson system, γ can be cleanly extracted by combining the CP violation measurements

$$\sin(-2\delta\gamma + \phi^{\rm s}_{\rm NP}) \sin(\Delta m_{\rm s} t) \quad \text{for} \quad J/\psi\,\phi \text{ (or } J/\psi\,\eta) \tag{10}$$

and

$$\sin(-2\delta\gamma + \phi^{\rm s}_{\rm NP} + \gamma) \sin(\Delta m_{\rm s} t) \quad \text{for} \quad D_s^+ K^- \text{ and } D_s^- K^+ \ .$$

Once γ is determined, ρ and η are given as

$$\rho = \frac{|V_{\rm ub}|}{\lambda|V_{\rm cb}|}\cos\gamma,\ \ \eta = \frac{|V_{\rm ub}|}{\lambda|V_{\rm cb}|}\sin\gamma\ ,$$

and β and $\delta\gamma$ are given by Equation 4. Now all the parameters of the CKM matrix are completely determined even if New Physics exists. Contributions from New Physics are then determined from Equations 9 and 10.

In this case, the allowed region of in $\tilde{\rho}$-$\tilde{\eta}$ plane given by the CP asymmetry measurement with B^0 and $\overline{B}^0 \to J/\psi\, K_S$ decays is no longer valid. What is measured from the asymmetry is not β, but $\beta + \phi^{\rm d}_{\rm NP}/2$. Similarly, the region given by the $\Delta m_{\rm d}/\Delta m_{\rm s}$ measurements is no longer valid since there could be sizeable contributions to Δm from New Physics in addition to the Standard Model box diagrams determining $|V_{\rm td}|$ and $|V_{\rm ts}|$. The only valid region in Figure 8 is that from the $|V_{\rm ub}|/(\lambda|V_{\rm cb}|)$ measurement. Then the apparent consistency seen in Figure 8 could be accidental. Once γ will be measured in the way explained above, the situation becomes clear. Figure 9 illustrates a possible situation when γ is measured with an accuracy of $\pm 5^\circ$. In this case, the theoretically clean determinations of γ outlined above will reveal New Physics.

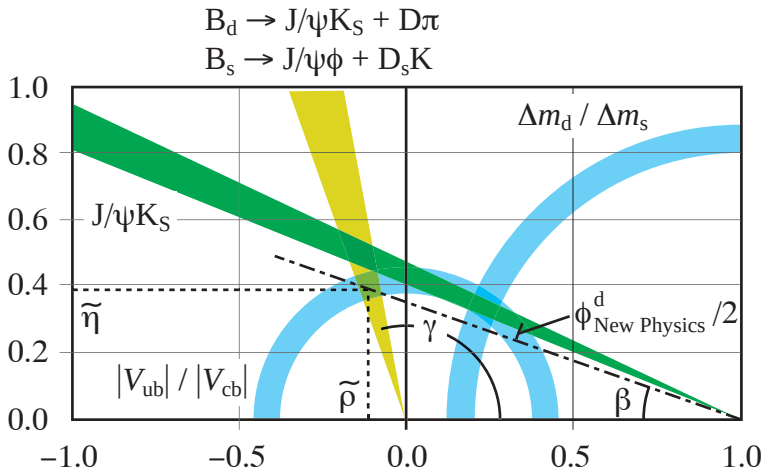

Figure 9: Possible situation of the allowed region in the $\tilde{\rho}$-$\tilde{\eta}$ plane in 2006

In the discussion above, we made an assumption that New Physics does not contribute to the decay amplitude, which may not be strictly true for

the $B^0 \to J/\psi\, K_S$ and $B_s^0 \to J/\psi\, \phi$ decays. Those decays do receive some contribution from the $b \to s$ penguin process where New Physics could appear in the loop. Whether New Physics indeed contributes to the $b \to s$ penguin process can be examined by studying CP violation in B^0 and $\overline{B}^0$ decaying into ϕK_S where the decays are generated only by the penguin processes. In the Standard Model, the process is dominated by a loop with the virtual top quark. Therefore, the phase of the decay amplitude is given by V_{ts}: i.e. the CP violation signature is given by

$$\sin(2\beta + \phi_{NP}^{d} - 2\delta\gamma + \phi_{NP}^{s-penguin}) \sin(\Delta m_d t) \ , \tag{11}$$

where $\phi_{NP}^{s-penguin}$ is the phase possibly introduced in the penguin processes by New Physics. By comparing the expressions given by Equations 9 and 11, we can examine whether New Physics contributes significantly to the $b \to s$ penguin processes.

New physics contribution to the $b \to d$ penguin processes can be studied from CP violation in B^0 and $\overline{B}^0$ decaying into $K^{*0}\overline{K}^{*0}$ or $\phi\pi^0$ where only the $b \to d$ penguin process contributes in the Standard Model.

Studies of $b \to s$ and $b \to d$ penguins can be made with the B_s meson system independently.

In conclusion, theoretically clean and model-independent determination of the parameters of the CKM matrix is possible even if there exists New Physics contributing to CP violation. Once the CKM parameters are determined, possible existence of New Physics could be cleanly established.

5 B Experiments at LHC

5.1 General Consideration

The goal of B physics in the LHC era [7] is to determine the CKM parameters in a model-independent way and to isolate the effect of New Physics so that its characteristics could be identified. This calls for an experiment capable of studying CP violation with both B^0 and B_s^0 systems decaying into various final states including those with only hadrons, with high statistics.

The production cross section of the $b\overline{b}$ quark pairs at the LHC energy is estimated to be $\sim$500 μb; far larger than at any existing machines. The fraction of events with b quarks, $\sigma_{b\overline{b}}/\sigma_{inelastic}$, is about 6×10^{-3} which is similar to the fraction of charm events in the present fixed-target charm

experiments. Thus, LHC appears to be a very promising place to perform high precision CP violation measurements in B-meson decays. At LHC, B_s, $\overline{B}_s$, $B_c^{\pm}$ and b-baryons are abundantly produced, in addition to $B^{\pm}$, B^0 and $\overline{B}^0$.

In order to exploit the potential of LHC, experiments need to have the following capabilities:

1. Trigger sensitive to both leptonic and hadronic final states.

2. Particle identification system capable of identifying p, K, π, μ and e within the required momentum range.

3. Vertex detector able to reconstruct primary and B vertices very precisely.

4. Tracking system with good momentum resolution.

In addition, a capability of reconstructing π^0 would enhance the potential of the experiment further.

ATLAS [8] and CMS [9] are two general purpose collider detectors designed to perform high p_T physics at LHC, such as studies of the top quark and search for the Higgs and supersymmetric particles in the central region of the pp interactions. As already demonstrated by CDF, general purpose collider experiments can cleanly reconstruct B-meson final states containing lepton pairs, such as $J/\psi\, K_S$, $J/\psi\phi$ and $\ell^+\ell^-$. Both ATLAS and CMS have an excellent muon and electron detection capability and a good vertex resolution, allowing them to collect a high statistics sample of such decays.

However, their first level high p_T lepton trigger is not sensitive to the hadronic final states. Hadronic decay modes can only be triggered by the semileptonic decay of the accompanying b hadrons. Due to the relatively small branching fraction for the semileptonic decay, the trigger efficiencies for hadronic decay modes will be low. The two experiments have no $p/K/\pi$ separation capability in the necessary momentum range. The energy loss, dE/dx, can be used for particle identification, but in a restricted momentum range with a modest accuracy. It is not sufficient to separate kaons from pions in the high momentum region relevant for the two-body decay modes of B mesons such as $\pi^+\pi^-$ and D_sK.

For those reasons, ATLAS and CMS will not be able to study CP violation with the final states necessary to perform model-independent analysis.

5.2 The LHCb Experiment

The LHCb detector [10] is designed to fulfill all four requirements listed above. Due to the trigger equally efficient for leptons and hadrons, the experiment will be able to exploit fully the physics potential of LHC at a much lower luminosity (2×10^{32} cm^{-2}s^{-1}) than the nominal luminosity (10^{34} cm^{-2}s^{-1}). Therefore, the experiment will be able to perform its full physics programme from the beginning of the LHC operation.

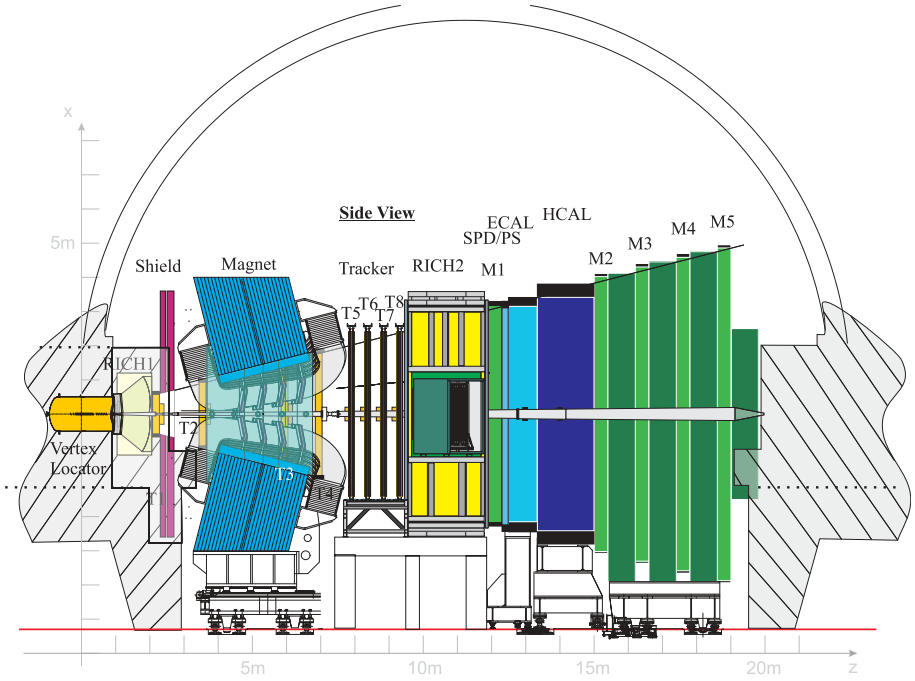

Figure 10: The LHCb spectrometer placed in the LHC Intersection-8 experimental area.

The detector layout shown in Figure 10 resembles a typical fixed target spectrometer. It consists of a vertex detector at the intersection point (placed in "Roman pots"). It followed by a tracking system, RICH counters with aerogel and gas radiators, a large-gap dipole magnet, a calorimeter system, and a muon system. An existing LEP experimental area is reused to install the detector. The interaction point is shifted by 11 m from the nominal point, the centre of the experimental hall, in order to accommodate the detector elements without extra excavation.

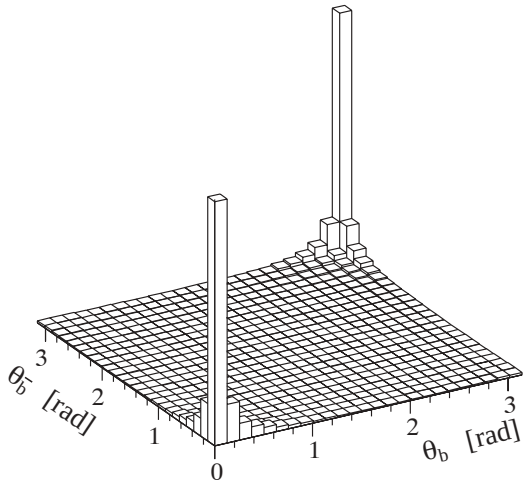

Figure 11: Polar angles of the b- and $\overline{\text{b}}$-hadrons obtained with the PYTHIA simulation programme.

The choice of the detector geometry is based on the fact that both the b- and $\overline{\text{b}}$-hadrons are predominantly produced in the same forward (or backward) cone at high energies. This is demonstrated in Figure 11 where the polar angles of the b- and $\overline{\text{b}}$-hadrons in one event obtained with the PYTHIA simulation programme are shown. The polar angle is defined with respect to the beam axis in the pp center-of-mass system. Detecting both b- and $\overline{\text{b}}$-hadron at the same time is essential for the flavour tag.

Further advantages of the forward geometry are:

- The b-hadrons produced in the forward direction are faster than those in the central region. Their average momentum is about 80 GeV/c, corresponding to a mean decay length of ~ 7 mm. Therefore, a good decay time resolution can be obtained for reconstructed B-mesons.

- The spectrometer can be built in an open geometry with an interaction region which is not surrounded by all the detector elements. This allows a vertex detector system to be built with sensors which can be extracted away from the beam during the injection using Roman Pot technique. During the data taking, the sensors are positioned close to the beam in order to achieve a good vertex resolution.

- In the forward region, momenta are mainly carried by the longitudinal

components. Therefore, the threshold value for the p_t trigger can be set low for electrons, muons and hadrons without being constrained by the detector requirements. This makes the p_t trigger more efficient than in the central region.

- The momentum range required for particle identification is well matched to the Ring Imaging Cherenkov Counters. The required size for the counters remains affordable.

- The open geometry allows easy installation, maintenance and possible upgrade.

It is also important to note that the detector covers the region of phase space which is not looked at by the two general purpose detectors.

A short description of the LHCb spectrometer follows.

- Beam Pipe
  A large vacuum tank with a length of 1.7 m and a diameter of 1 m is placed around the interaction point to accommodate the vertex detector system with its retraction mechanics. It has a 2 mm Al forward exit window over the full detector acceptance. This part is followed by two conical sections; the first one is 1.4 m long with a 25 mrad opening angle, and the second part is 16 m long with a 10 mrad opening angle. Except bellows and flanges and the last 6.3 m of the 10 mrad cone, the beam pipe is made from Al-Be alloy in order to reduce the radiation length. This is essential for minimising the occupancies of the tracking and RICH systems, as well as for the detection of photons and electrons.

- Magnet
  A dipole magnet with Al conductor provides a field integral of 4 Tm. The polarity of the field can be changed to reduce systematic errors in the CP-violation measurements that could result from a left-right asymmetry of the detector. The two pole faces form a wedge shape following the spectrometer acceptance, in order to reduce the power consumption.

- Vertex Locator (VELO)
  A total of 27 stations of silicon microstrip detectors are placed perpendicular to the beam of which 25 stations are used as a vertex detector

system. The remaining two stations are dedicated for detecting bunch crossings with more than one pp interaction as a part of Level-0 trigger (pile-up veto counter). Stations are split into two halves, covering the left and right 180° sections. One vertex detector station consists of two Si sensor planes with different strip layouts, one for r and the other for ϕ measurements. The pile-up veto counter has only r measurement sensors. Signals are read-out and stored in analog pipeline buffers in every bunch crossing, i.e. 25 nsec. The closest distance between the active silicon area and the beam is 8 mm. In order to cope with high radiation dose expected at this position so close to the beam, n-on-n silicon sensors are taken as baseline. The silicon detectors are placed in Roman pots with 250 μm thick aluminium foil, which acts as a shield against RF pickup of the circulating beam bunches. In order to avoid collapse, a secondary vacuum is maintained inside the Roman pots. During the injection and acceleration, the Roman pot system will be moved away from the beam to avoid interference with the machine operation and accidental irradiation of the detectors.

- Tracking
  Because of the high particle density close to the beam pipe, the LHCb tracking detector is split into inner and outer systems. The boundary between the two was chosen so that the occupancy of the outer tracker does not exceed 15% at the highest point. The outer tracking system uses drift chambers based on a straw cells structure. Straws are made by winding the carbon-loaded Kapton foil. The diameter of the straw is 5 mm and drift-time is sampled over 50 nsec, i.e. two bunch crossings. The inner tracking system is made from single sided p-on-n Si strip detectors with a strip pitch of $\sim$200 μm. Since the sensitive regions of the Si sensor are further away from the beam ($>$ several centimeters) compared with the sensor for the Vertex Locator, the problem of radiation damage is less severe.

- RICH
  The RICH system of the LHCb detector consists of two detectors with three different radiators in order to cover the required momentum range, 1–100 GeV/c. The first detector uses aerogel and C_4F_{10} gas as radiators. The second detector, responsible for high momentum particles, is placed after the magnet and uses CF_4 as radiator. The

Cherenkov light is detected with planes of Hybrid Photon Detectors (HPD's) placed outside the spectrometer acceptance.

- Calorimeters
  The calorimeter system consists of a preshower detector followed by electromagnetic and hadronic calorimeters. It also serves as the initial part of the muon filter system. The cells of the Preshower detector are made as two scintillator plates sandwiching 14 mm-thick lead plates. The cell size of the preshower detector is matched to the module size of the electromagnetic calorimeter. For the electromagnetic part a Shashlik calorimeter is used since a modest energy resolution is required. The hadron calorimeter is based on a scintillating tile design similar to that used in the ATLAS experiment with a reduced energy resolution.

- Muon
  For the muon stations Resistive Plate Chambers are used in the region where the charged particle rate is below 1 kHz/cm^2. For the region with a charged particle rate from 1 kHz/cm^2 to 100 kHz/cm^2, Multi Wire Proportional Chambers (MWPC's) are used. For the small region of the first muon station closed to the beam pipe, where the charged particle rate exceeds 100 kHz/cm^2, triple-GEM chambers or MWPC's with asymmetric gas gap are being considered.

- Trigger
  The LHCb trigger is divided into four decision levels. The Level-0 decision is based on high-p_{T} hadrons, electrons or γ found in the calorimeter system or muons found in the muon system. Information on those candidates are sent to the Level-0 Decision Unit. The number of primary vertex candidates is determined using the pile-up veto counters in the Vertex Locator and sent also to the Level-0 Decision Unit. Based on all the information, the Level-0 Decision Unit makes an over-all Level-0 decision. Events with multiple pp interactions are discarded. Rejection of background in the reconstructed final states and obtaining a correct flavour tag are much more difficult in those events. The Level-0 trigger provides a modest reduction of minimum bias events by a factor of $\sim$10. At Level-1, data from the vertex detector are used to select events with multiple vertices. In addition, those p_{T} measurements made by Level-0 can be combined with the tracks having large impact parameter found in the Vertex Locator. This provides a further reduction of

the event rate. Level-1 provides a reduction factor of ∼25 for minimum bias events. After a positive decision of the Level-1 trigger, data are read out to an event buffer. Hereafter, all the detector information is in principle available for the trigger decision. At Level-2, a further enhancement of events with b-hadrons is achieved by combining different detector components: e.g. by adding momentum information from the main tracking system to the impact parameter calculation with the Vertex Locator. At Level-3, the trigger decision is made by reconstructing the decays.

5.3 Important Characteristics of the LHCb Detector

The benefit of having particle identification and good invariant mass resolution can be best demonstrated by reconstructing $B_s \to D_s^+ K^-$ decays. The worst background to this decay mode comes from $B_s \to D_s^+ \pi^-$ decays which are used to study B_s-$\overline{B}_s$ oscillations. Compared to this decay mode, the branching fraction of $B_s \to D_s^+ K^-$ is suppressed by a factor of $1/\lambda^2 \approx 20$. The two decay modes have an identical decay topology, thus only the invariant mass resolution and particle identification can help to reduce this background. It should be noted that momenta of K^- and π^- from these decay modes are large since they are two-body decays.

Figure 12 shows the reconstructed invariant mass distributions expected with the LHCb detector for $D_s^+ K^-$ combinations without and with particle identification using RICH. With the combination of the good mass resolution ($\sigma = 11$ MeV/c^2) and RICH particle identification, the background from $B_s \to D_s^+ \pi^-$ decays can be almost completely removed in the reconstructed $D_s^+ K^-$ sample. It should be noted that no CP violation effect is expected in the background decay mode. The decay time resolution is found to be 40 fsec.

The LHCb trigger system is designed to cope with the rather small $\sigma_{b\bar{b}}/\sigma_{\text{inelastic}}$ of $\sim 6 \times 10^{-3}$ at the LHC energies, still maintaining a high efficiency for events with b hadrons. The strategy is to spread the suppression factors evenly and not to rely on a particular trigger selection, in particular at early levels where available information from the detector is limited. This reflects in the modest suppression factors of 10 and 25 for the ordinary pp interaction events by the Level-0 and Level-1, respectively. Simulation results of the trigger performance can be relied upon for such a modest suppression. By not heavily relaying on a particular selection criterion, the trigger system

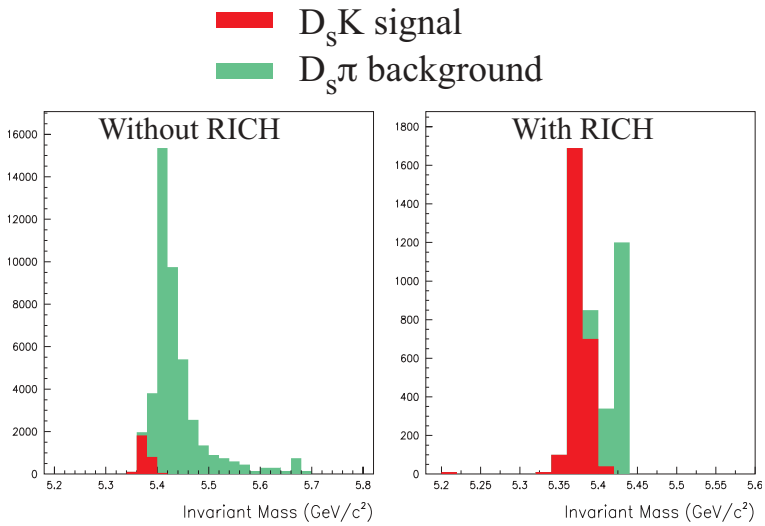

Figure 12: The LHCb simulation results for the reconstructed invariant mass distributions for $D_s^+K^-$ combinations without and with particle identification using RICH.

is flexible and can be readjusted to the yet unknown running conditions of the experiment.

With the particle identification capability, an efficient flavour tag can be obtained using the charged kaons from the b hadron decays. No lepton is required in the analysis for flavour tagging. Therefore, the Level-0 hadron high p_T trigger increases significantly the statistics of the sample with pure hadronic B decay final states compared with the lepton high p_T trigger alone. Table 1 summarises the Level-0 trigger efficiencies for various decay modes. Efficiencies are calculated for those events where the initial flavour is identified and the final state is fully reconstructed with all the cuts applied to remove background. While $J/\psi K_S$ final states are mainly triggered by the muon and electron high-p_T triggers, the hadron high-p_T trigger is essential for the hadronic final states.

The table also indicates that the Level-0 trigger efficiencies are very high for those events useful in the analysis. As a result, the LHCb experiment will run with a luminosity of 2×10^{32} cm^{-2}s^{-1} and still collect 2.4 k reconstructed and initial flavour tagged B_s and $\overline{B}_s$ decays into $D_s^+K^-$ and $D_s^-K^+$ in one year. With this statistics, γ can be measured with an accuracy of $\sim 10°$. By combining the result from the decays of B^0 and $\overline{B}^0$ into $D^{*+}\pi^-$ and $D^{*-}\pi^+$,

Table 1: Level-0 trigger efficiencies for reconstructed and flavour tagged final states.

Decay Mode	Level-0 high-p_T			Level-0
	muon	electron	hadron	all combined
$B^0 \to J/\psi(e^+e^-)K_S$	0.17	0.63	0.17	0.72
$B^0 \to J/\psi(\mu^+\mu^-)K_S$	0.87	0.06	0.16	0.88
$B_s \to D_s^+K^-$	0.15	0.09	0.45	0.54
$B^0 \to \pi^+\pi^-$	0.14	0.08	0.70	0.76

γ will be measured with a precision of better than 7° with one year of data taking.

At this luminosity, the bunch interactions are dominated by events with only one pp collision. The running luminosity will be locally tuned at the LHCb intersection such that the experiment can run with this optimal luminosity while the other LHC experiments run at the design luminosity. It must be noted that running at lower luminosities has an additional benefit: the radiation damage of the detector is reduced.

6 Conclusions

CP violation outside of the neutral kaon system has been observed for first time by BABAR and BELLE experiments in the decay of B^0 and $\overline{B}^0$ into the $J/\psi\, K_S$ final state. Current analysis shows that all the measurements related to b hadron decays are consistent with the CKM picture, including CP violation. Although BABAR, BELLE, CDF and D0 will further enhance the study in near future, a new generation of experiment at LHC is needed in order to examine the CKM picture in a model-independent way. It should be noted that a dedicated experiment at the Tevatron [11] would have a similar performance. LHCb, a dedicated detector for B physics at LHC with particle identification capability and trigger sensitive to both leptonic and hadronic final states, should be able to study CP violation in both B^0 and B_s^0 meson systems in many decay modes. Some of those decay modes are essential to determine the CKM parameter in a theoretically clean model-independent way. And this will also allow the effect of possible New Physics to be identified unambiguously.

Acknowledgments

I thank the organizers of the school for their hospitality and creating a stimulating environment. R. Forty and O. Schneider are deeply acknowledged for many useful comments and suggestions on this manuscript.

References

[1] Kobayashi, M. and Maskawa, K. (1972), *Prog. Theor. Phys.* **49**, 282.

[2] Shaposhnikov, M.E. (1986), *JETP Lett.* **44**, 364.

[3] Groom, D.E. et al. [Particle Data Group] (2000), *The European Physical Journal* **C15**, 1.

[4] Wolfenstein, L. (1983), *Phys. Rev. Lett.* **51**, 1945.

[5] Hagelin, J. S. (1981), *Nucl. Phys.* **B193**, 123,
More details, see Buras, A. J, (1999), *Proceedings of 14th Lake Louise Winter Institute* (Singapore: World Scientific).

[6] Aubert, B. et al (2001), *Phys. Rev.Lett.* **87**, 091801.
Abe, K. et al (2001), *Phys. Rev.Lett.* **87**, 091802.

[7] Ahmadov, A. et al (2000) *Proceedings of the Workshop on Standard Model Physics (and more) at the LHC*, **CERN 2000-04** .

[8] Armstrong, W. W. (1994), *ATLAS Technical Proposal*, **CERN/LHCC/94-43**.

[9] Bayatian, G. L. (1994), *CMS Technical Proposal*, **CERN/LHCC/94-38**.

[10] Amato, S. (1998), *LHCb Technical Proposal*, **CERN/LHCC/98-4**.

[11] Kulyavtsev, A. (2000), *BTeV Proposal*, **BTeV-doc-66-v1**.